0026-895X/11/8005-879–888$25.00
MOLECULAR PHARMACOLOGY
Vol. 80, No. 5
72124/3723164
Mol Pharmacol 80:879–888, 2011
Printed in U.S.A.

Application of Homology Modeling to Generate CYP1A1 Mutants with Enhanced Activation of the Cancer Chemotherapeutic Prodrug Dacarbazine[S]

Benjamin C. Lewis, Peter I. Mackenzie, and John O. Miners

Department of Clinical Pharmacology, School of Medicine, Flinders University, Adelaide, Australia

Received March 6, 2011; accepted August 3, 2011

ABSTRACT

The chemotherapeutic prodrug dacarbazine (DTIC) has limited efficacy in human malignancies and exhibits numerous adverse effects that arise from systemic exposure to the cytotoxic metabolite. DTIC is activated by CYP1A1 and CYP1A2 catalyzed N-demethylation. However, structural features of these enzymes that confer DTIC N-demethylation have not been characterized. A validated homology model of CYP1A1 was employed to elucidate structure-activity relationships and to engineer CYP1A1 enzymes with altered DTIC activation. In silico docking demonstrated that DTIC orientates proximally to Ser122, Phe123, Asp313, Ala317, Ile386, Tyr259, and Leu496 of human CYP1A1. The site of metabolism is positioned 5.6 Å from the heme iron at an angle of 105.3°. Binding in the active site is stabilized by H-bonding between Tyr259 and the N^2 position of the imidazole ring. Twenty-seven CYP1A1 mutants were generated and expressed in *Escherichia coli* in yields ranging from 9 to 225 pmol P450/mg. DTIC N-demethylation by the E161K, E256K, and I458V mutants exhibited Michaelis-Menten kinetics, with decreases in K_m (183–249 μM) that doubled the catalytic efficiency ($p < 0.05$) relative to wild-type CYP1A1 (K_m, 408 ± 43 μM; V_{max}, 28 ± 4 pmol · min^{-1} · pmol of P450^{-1}). The generation of enzymes with catalytically enhanced DTIC activation highlights the potential use of mutant CYP1A1 proteins in P450-based gene-directed enzyme prodrug therapy for the treatment of metastatic malignant melanoma.

Introduction

The chemotherapeutic prodrug dacarbazine (DTIC; Fig. 1) is the most effective single agent used for the treatment of malignant melanoma. However, a beneficial response to DTIC treatment occurs only in approximately 19% of patients (Luce et al., 1970). During the past 20 years, all compounds in phase III clinical trials targeted to treat metastatic melanoma have failed to improve patient outcomes compared with DTIC (Erdmann, 2010). DTIC requires metabolic activation by cytochromes P450 1A1, 1A2 and, to a much lesser extent, 2E1 for cytotoxicity (Reid et al., 1999). The main metabolic pathway involves α-hydroxylation of one of the *N*-methyl groups by the P450 enzymes to form 5-(3-hydroxymethyl-3-methyl-triazen-1-yl)-imidazole-4-carboxamide (Fig. 1). This metabolite is chemically unstable, losing formaldehyde to generate the *N*-demethylated species 5-(3-methyl-triazen-1-yl)-imidazole-4-carboxamide (Rooseboom et al., 2004; Sanada et al., 2004). Rapid decomposition of 5-(3-methyl-triazen-1-yl)-imidazole-4-carboxamide yields 5-aminoimidazole-4-carboxamide (AIC), the major metabolite detected in plasma and urine, and the reactive species methane diazohydroxide, which produces molecular nitrogen and the methyl cation responsible for the formation of *O*-alkylguanine-DNA adducts (Meer et al., 1986).

Efforts to improve DTIC activation have focused on the development of new chemical analogs such as temozolomide (Stevens et al., 1987). Like DTIC, however, the activated metabolite requires transfer to the tumor via the circulation, thus resulting in systemic exposure. Containment of the cytotoxic metabolites in the tumor environment would potentially reduce the adverse effects experienced by patients during conventional chemotherapy with DTIC. As a targeted approach to chemotherapy, gene-directed enzyme prodrug therapy (GDEPT) (Aghi et al., 2000; Ferguson et al., 2001; Xu and McLeod, 2001; Baldwin et al., 2003; Daly, 2003; Denny, 2003) offers a strategy to improve tumor/drug selectivity in

This work was supported by the National Health and Medical Research Council of Australia and the Faculty of Health Sciences of Flinders University.
Article, publication date, and citation information can be found at http://molpharm.aspetjournals.org.
doi:10.1124/mol.111.072124.
[S] The online version of this article (available at http://molpharm.aspetjournals.org) contains supplemental material.

ABBREVIATIONS: DTIC, dacarbazine [5-(3,3-dimethyl-triazenyl)-imidazole-4-carboxamide]; P450, cytochrome P450; AIC, 5-aminoimidazole-4-carboxamide; GDEPT, gene-directed enzyme prodrug therapy; CPR, cytochrome P450 NADPH oxidoreductase; HPLC, high-performance liquid chromatography; RMSD, root-mean-square deviation.

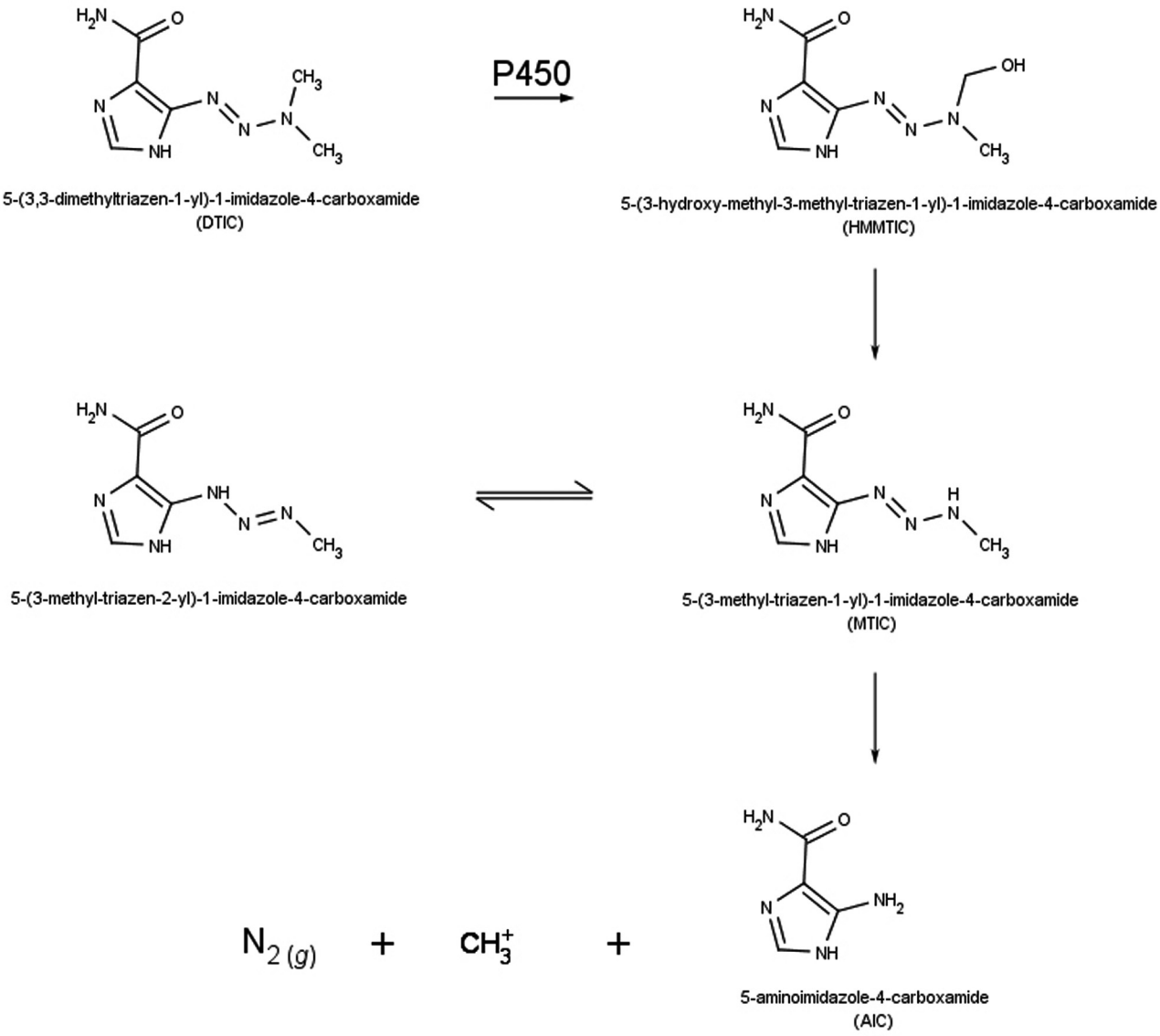

Fig. 1. Metabolic activation of dacarbazine (DTIC).

the treatment of cancer. GDEPT functions by localizing activation of a systemically administered prodrug by using the expression of an exogenous drug-activating enzyme targeted to the tumor environment. The gene(s) encoding the enzyme(s) should be of human origin to alleviate adverse immune responses and should be expressed in negligible levels throughout the body to avoid nonspecific formation of the cytotoxic metabolite (Denny, 2003). The protein must achieve sufficient expression in the tumors and have high catalytic efficiency (Daly, 2003). Although the results from preclinical trials are encouraging with respect to the vectors and promoters used for gene expression (Kan et al., 2001; Löhr et al., 2001), improvements in the efficiency of the therapeutic enzymes used in GDEPT is still required.

An understanding of the structural organization and chemical interactions between P450 enzymes and their respective substrates is pivotal for characterizing structure-activity relationships. In the absence of a human CYP1A1 crystal structure, structure-activity analyses have been essential in understanding the mechanisms responsible for the substrate selectivity, regioselectivity, and stereoselectivity of this enzyme (Miles et al., 2000; Ridderström et al., 2001; Lewis et al., 2002, 2004; Lewis, 2003; Liu et al., 2004; Schwarz et al., 2004; Ericksen and Szklarz, 2005). More recently, targeted mutagenesis experiments have been directed by in silico approaches based on the X-ray crystal structures of the human P450 enzymes. In a previous study, we used the human CYP1A2 X-ray crystal coordinates as a structural template for generating a chemically and energetically valid CYP1A1 homology model (Lewis et al., 2007). The predictivity of the CYP1A1 model was confirmed using directed mutagenesis, which identified the active-site residues responsible for the productive orientation and binding of 7-ethoxyresorufin.

Here, the CYP1A1 homology model was employed to direct the structural modification of this enzyme to increase its catalytic efficiency (V_{max}/K_m) for DTIC N-demethylation and subsequent activation. E161K, V228T, E256K, and I458V substitutions in human CYP1A1 were demonstrated to enhance activation of DTIC via the N-demethylation pathway, primarily by decreasing the K_m for this reaction.

Materials and Methods

Chemicals and Reagents. Restriction enzymes were purchased from New England Biolabs, Inc. (Hitchin, Hertfordshire, UK), DTIC and AIC were purchased from Sigma-Aldrich (Sydney, NSW, Australia), and *Escherichia coli* DH5α cells from Life Technologies (Melbourne, VIC, Australia). Gel-purified oligonucleotides were supplied by Sigma-Genosys (Sydney, NSW, Australia), Pfu Ultra HS II Polymerase by Stratagene (La Jolla, CA), and shrimp alkaline phosphatase by Roche Diagnostics GmbH (Penzberg, Germany). All other chemicals and reagents were of analytical grade and purchased from Sigma-Aldrich unless otherwise stated.

In Silico Modeling to Identify Sites for Targeted Mutagenesis. Homology models containing mutations were constructed using the wild-type CYP1A1 homology model generated previously (Lewis et al., 2007). Targeted residues were mutated in silico, incorporating the desired amino acid. Each substituted residue was energy minimized as a subset of the entire protein molecule using the Powell conjugate gradient method with an energy cutoff set to 0.05 kcal $\cdot$ mol^{-1} $\cdot$ Å^{-1}. A "hot region" of 6 Å surrounding the substituted residue was established in which the side chains of all residues were minimized. A further "intermediate region" of 12Å was generated to set the minimization environment without side-chain movement. Minimization by this method allowed changes in the energetic forces experienced by residues that either adjoin or neighbor the substituted amino acid.

Automated docking was achieved using the FlexX docking suite (SYBYL 7.3; Tripos, St. Louis, MO). Docking of the ligand was consensus scored (CScore) based on its interactions with the protein and the key residues involved in binding and orientation of DTIC in the protein active site. Distance and angle data were collected to characterize the orientation of docked substrate poses. Distances were measured between the α-carbon of the substrate (i.e., the site of hydroxylation that precedes demethylation) and the heme iron. Angles (θ) were between the N1 atom of the heme pyrrole proximal to the I-helix, the heme iron, and the α-carbon of the substrate. Active-site residues involved in the binding and orientation of DTIC were targeted based on their proximity to the docked DTIC molecule generated in silico. Residues within a 3-Å radius in which side-chain chemistry interacted with the docked substrate were considered for mutagenesis. In addition, residues able to affect the electrostatic environment surrounding the heme, the reductase binding domain, and residues potentially involved in the metabolism of heterocyclic amines in rat CYP1A1 were targeted. All substitutions were guided by consideration of the importance of the side-chain functional group(s) and how they contribute to substrate alignment, orientation, and enzyme function.

CYP1A1 and CPR cDNAs, and Generation of CYP1A1 Mutants. N terminus modifications previously shown to promote high levels of bacterial expression of human P450s were made to the wild-type CYP1A1 cDNA (GenBank accession no. NM_000499) as described previously (Lewis et al., 2007). NdeI and XbaI restriction sites (shown in bold) were additionally incorporated for cloning purposes: forward primer, 5′-AT**CATATG**ATCATGGCTCTGTTATTAGCAGTTTTTCTGTTCTGTCTGG-3′; reverse primer, 5′-TA**TCTAGA**ACCTAGTGATGGTGATGGTGATGAGAGCGCAGCTGCATTTGG-3′. The 1551-base pair polymerase chain reaction product was ligated into the pCW ori(+) plasmid and transformed into DH5α *E. coli* cells. The CPR expression construct, generated using the bacterial plasmid pACYC, comprised the OmpA signal sequence fused upstream of the full-length native rat CPR sequence (Shen et al., 1989).

The CYP1A1 residues Ser116, Ser122, Phe123, Glu161, Glu166, Val191, Phe224, Val228, Glu256, Tyr259, Asn309, Leu312, Asp313, Gly316, Ala317, Asp320, Thr321, Val322, Ile386, Ile458, and Thr497 were mutated to generate 116Ala, 122Ala, 122Thr, 123Ala, 161Lys, 166Gln, 191Met, 224Ala, 228Thr, 256Lys, 259Phe, 309Thr, 312Phe, 313Ala, 313Asn, 316Val, 317Gly, 317Tyr, 320Ala, 321Gly, 321Pro, 321Ser, 322Ala, 386Gly, 386Val, 458Pro, 458Val, and 497Ser variants. Supplemental data (video 1) displays all sites of mutagenesis relative to the tertiary structure of human CYP1A1. Because of the high GC content of the CYP1A1 cDNA, the primer design method described by Zheng et al. (2004) was used to minimize primer heterodimerization. The partially overlapping primers used for mutagenesis are given in Table 1; cycling parameters were as described elsewhere (Lewis et al., 2007). Mutations were confirmed by nucleotide sequencing on both strands (ABI 3130-XL DNA sequencer; Applied Biosystems, Victoria, NSW, Australia).

Heterologous Coexpression of P450s and CPR. The wild-type pCW 17α-CYP1A1 and all CYP1A1 mutant (Table 1) cDNAs were individually transformed into DH5α *E. coli* cells that were stably transformed with the pACYC OmpA-rCPR construct as described previously (Lewis et al., 2007). Cells cultured overnight (5 ml) in Luria-Bertani broth with ampicillin (100 μg/ml) and chloramphenicol (10 μg/ml) at 37°C were used to inoculate 100-ml cultures of Terrific broth containing

TABLE 1
Primers used for site-directed mutagenesis
Mutagenic nucleotides are underlined. Wild-type CYP1A1 (GenBank accession NM_000499) was used as the parent template to generate all mutants.

CYP1A1 Mutant	Primer Overlap (5′ forward to 5′ reverse)
S116A	CCCTCATCGCTAATGGTCAGAGCATGTCC
	GTGGAAGTGGGAGTAGCGATTACCAG
S122A	CAGAGCATGGCCTTCAGCCCAGACTCTGG
	GTCATTACCAGTCTCGTACCGGAAGTCG
S122T	CAGAGCATGACCTTCAGCCCAGACTCTGG
	GTCATTACCAGTCTCGTACTGGAAGTCG
F123A	GCATGTCCGCCAGCCCAGACTCTGGACC
	CATTACCAGTCTCGTACAGGCGGTCGGGTC
E161K	CCTCAACCTCCTGCTACCTGGAAAAGCATGTGAGCAAGGAGG
	GGAGTTGGAGGACGATGGACCTTTTTCGTACACTCGTTCCTCC
E166Q	GGAAGAGCATGTGAGCAAGCAGGCTGAGGTCCTGATAAGC
	CCTTCTCGTACACTCGTTCGTCCGACTCCAGGACTATTCG
V191M	CTTTAACCCCTACAGGTATGTGATGGTATCAGTGACCAATG
	GAAATTGGGGATGTCCATACACTACCATAGTCACTGGTTAC
F224A	GAATAATAATGCCGGGGAGGTGGTTGGCTC
	GGATCAGTTGGACTTATTATTACGGCCCCTCC
V228T	GGGAGGTGACTGGCTCTGGAAACCCAGC
	CTTATTATTAAAGCCCCTCCACTGACCGAGAC
E256K	ACCTGAATAAGAAGTTCTACAGCTTC
	CGGAAGTTCCTGGACTTATTCTTCAAG
Y259F	GAAGTTCTTCAGCTTCATGCAGAAGATG
	GGACTTACTCTTCAAGAAGTCGAAG
N309T	GATCATTACCATCGTCTTGGACCTCTTTGG
	CAGTCTACTCTTCTAGTAATGGTAGCAGA
L312F	CATCGTCTTTGACCTCTTTGGAGCTGGG
	CTAGTAATTGTAGCAGAAACTGGAGAA
D313A	CGTCTTGGCCCTCTTTGGAGCTGGGTTTGAC
	CTCTTCTAGTAATTGTAGCAGAACCGGGAGAAACC
D313N	AGATCATTAACATCGTCTTGAACCTCTTTGGAGCTGGG
	TCTAGTAATTGTAGCAGAACTTGGAGAAACCTCGACCC
G316V	TCTTTGTAGCTGGGTTTGACACAG
	GCAGAACCTGGAGAAACATCGACCC
A317G	CTTTGGAGGTGGGTTTGACACAGTC
	GCAGAACCTGGAGAAACCTCCACCCAAAC
A317Y	TCTTTGGATATGGGTTTGACACAGTCAC
	GCAGAACCTGGAGAAACCTATACCCAAAC
D320A	GGTTTGCCACAGTCACAACTGCTATCTC
	CTGGAGAAACCTCGACCCAAACGGTGTCAGTG
T321G	GGTTTGACGGAGTCACAACTGCTATCTCC
	GGAGAAACCTCGACCCAAACTGCCTCAGTGTTG
T321P	CTGGGTTTGACCCAGTCACAACTGCTATCTCC
	CTGGAGAAACCTCGACCCAAACTGGGTCAGTG
T321S	GGTTTGACTCAGTCACAACTGCTATCTCC
	GGAGAAACCTCGACCCAAACTGAGTCAGTG
V322A	GACACAGCCACAACTGCTATCTCC
	CTCGACCCAAACTGTGTCGGTGTTGAC
I386G	CCTTCACCGGCCCCCACAGCACAACAAGAG
	GAAGGAAGCAGGGGAAGTGGCCGGGGGTGT
I458P	GGGCAAGCGGAAGTGTCCCGGTGAGACCATTGCCCG
	CCCGTTCGCCTTCACAGGGCCACTCTGGTAACGGGC
I458V	GGCAAGCGGAAGTGTGTCGGTGAGACCATTGCCCGC
	CGTACCCGTTCGCCTTCACACAGCCACTCTGGTAACGGGCG
T497S	GGGCTATCCATGAAGCATGCCTGC
	GGGGGTAGATACCCGATAGGTACTTC

100 μg/ml ampicillin, 10 μg/ml chloramphenicol, and rare elements solution (25 μM $FeCl_3 \cdot 6H_2O$, 2 μM $ZnCl_3 \cdot 4H_2O$, 2.5 μM $CaCl_2 \cdot 6H_2O$, 2.5 μM Na_2MoO_4, 1.7 μM $CaCl_2 \cdot 2H_2O$, 1.85 μM $CuCl_2$, 2 μM H_3BO_3, and 30 μM HCl). Cultures were grown at 37°C with shaking (160 rpm) for 4 h or until reaching an optical density of 0.7 to 0.9 AU at 600 nm. After cooling to 26°C, cultures were induced with isopropyl-1-thio-β-D-galactopyranoside (1 mM) and δ-aminolevulinic acid (1 mM) and then grown at 26°C with shaking (160 rpm) for an additional 64 h in <1% dissolved oxygen. Membrane fractions were prepared according to Gillam et al. (1993) and stored in aliquots at −80°C. Protein concentrations were determined using the method of Lowry et al. (1951). Total P450 content and CPR activity were measured spectrophotometrically (Omura and Sato, 1964a,b; Yasukochi and Masters, 1976).

Measurement of DTIC N-Demethylation Activity. AIC formation was determined in opaque glass tubes at 37°C in a total incubation volume of 0.2 ml. Incubation mixtures contained coexpressed CYP1A1 (5.0 pmol) and CPR (5–160 pmol), NADPH generating system (1 mM $NADP^+$, 10 mM glucose 6-phosphate, 2 IU of glucose-6-phosphate dehydrogenase, and 5 mM $MgCl_2$), and DTIC (100–6000 μM) in phosphate buffer (0.1 M, pH 7.4). After a 5-min preincubation at 37°C in a shaking water bath, reactions were initiated by the addition of NADPH generating system. Incubations were terminated after 60 min by the addition of 2 μl of ice-cold 70% perchloric acid. Reaction mixtures were vortex-mixed, cooled on ice for 10 min, centrifuged (5000*g* for 10 min at 4°C), and an aliquot (20 μl) of the supernatant fraction was injected onto the HPLC column.

DTIC stock solutions were prepared in a 1:1 M ratio of HCl in water and protected from light. Dilutions of the DTIC stock solutions were confirmed by HPLC to ensure linearity; r^2 values were >0.991. Samples were prepared by diluting 1:100 with mobile phase, and an aliquot (4 μl) was injected onto the HPLC column and separated using a mobile phase comprising 80% A and 20% B (see *Measurement of AIC Formation*). Elution was monitored by UV detection at 267 nm. The retention time of DTIC was 1.4 min at a mobile phase flow rate of 1 ml/min.

Measurement of AIC Formation. AIC was separated using a Waters Nova-Pak C18 column (150 × 3.9 mm, 4 μm; Waters Corporation, MA) consisting of mobile phase A, 10 mM heptane sulfonic acid, 5% (v/v) acetonitrile, and 0.1% (v/v) triethylamine, adjusted to pH 3.0 with 85% orthophosphoric acid (filter sterilized; 0.45 μm), and mobile phase B, acetonitrile (100%). The following mobile phase gradient was used to elute AIC: 100% A held for 5.1 min, then changed to 70% A/30% B over 0.7 min, and held for 0.1 min, followed by returning to 100% A over 0.1 min and held for 5.1 min. AIC was monitored by UV detection at 267 nm. The retention time of AIC was 5.2 min using a mobile phase flow rate of 1 ml/min. Unknown concentrations of AIC were determined by comparison of the peak area to a calibration curve constructed in the concentration range 2.5 to 100 μM.

Calculation of DTIC Kinetic Parameters. The rates of AIC formation versus substrate concentration (100–6000 μM) were model-fitted using the nonlinear curve fitting program EnzFitter (Biosoft, Cambridge, UK). Kinetic constants [K_m, V_{max}, the Hill coefficient (n_H), and the substrate concentration at half the maximum velocity (S_{50})] for AIC formation were derived from fitting either the Michaelis-Menten equation or the Hill equation to experimental data. Goodness of fit was assessed from the *F* statistic, 95% confidence intervals, r^2 value, and standard error of the parameter fit. Statistical analysis (multivariate general linear model; Tukey post hoc) was undertaken using PASW Statistics version 18.0 (SPSS Inc., Chicago, IL). Kinetic data are given as the mean ± S.D. of four separate experiments, with values of $p < 0.05$ considered significant.

Results

Automated Docking of DTIC. DTIC was docked into the CYP1A1 active-site using the homology model generated previously in this laboratory (Lewis et al., 2007). The energetically favored pose of DTIC places the α-carbon of the side-chain *N*-methyl at 5.6 Å from the iron at an angle of 105.3° perpendicular to the plane of the heme (Fig. 2A). This measurement is dependent on free rotation about the *N*-dimethyl side-chain of the triazene of DTIC. Binding and orientation of DTIC within the active-site involves Ile115, Ser120, Ser122, Phe123, Phe224, Phe258, Tyr259, Asp313, Gly316, Ala317, Ile386, and Leu496, with all twelve residues positioned within a 3-Å radius from DTIC (Fig. 2B). Van der Waals forces between enzyme and substrate suggest significant interactions with Ser122, Phe123, Asp313, Ala317, Ile386, Tyr259, and Leu496. H-bonding can occur between the oxygen of Ser122 and the triazene N^6 nitrogen of DTIC. However, based on the speciation of DTIC at pH 7.4, H-bonding at this location is unlikely unless the active-site pH drops below 4 during substrate binding or catalysis. Further H-bonding is observed between the hydroxyl hydrogen of Tyr259 and the N^2 aromatic nitrogen of the imidazole ring, which is likely to occur in all substrate molecules at physiological pH. Edge-to-face and parallel displaced aromatic interactions are predominant with Phe123, and Phe224, Phe258, and Tyr259, respectively (Fig. 2B). The free rotation of the *N*-dimethyl substituent of DTIC seems dependent on the size of residues located at positions 317 (I-helix; SRS 4) and 386 (K-helix/β2-3 loop; SRS5). Residue 317 is a small nonpolar aliphatic alanine and residue 386 is a Cβ-branched nonpolar aliphatic isoleucine. These two residues constrain the width of the catalytic cleft of the active-site to 5.4 Å. Aspartate 313 is near the aromatic nitrogen closest to the triazene substituent. At pH 7.4, this nitrogen is negatively charged in 97% of DTIC molecules. Thus, strong charge interactions contributed by Asp313 may affect the orientation of DTIC in the CYP1A1 active-site.

Mutant CYP1A1 Enzymes. Structural models were built to assist interpretation of the mutagenesis data. Table 2 displays the angle and distance data for DTIC docked in silico for each mutant orientated for productive *N*-demethylation. The root-mean-square deviation (RMSD) of each mutant was calculated relative to the wild-type model to identify structural differences. Substitutions generating the greatest structural deviations relative to wild-type are represented by large RMSD values. Of particular interest were RMSD values for S116A, F224A, V228T, Y259F, and T497S, which show structural deviations are dependent on amino acid chemistry (i.e., polar, aliphatic, aromatic, charge state) and the spatial orientation of residues relative to neighboring amino acids (Table 2).

Heterologous Coexpression of P450s. Wild-type CYP1A1 and mutant CYP1A1 enzymes were individually coexpressed with CPR. The expression of holoenzyme achieved in *E. coli* ($n \geq 3$ experiments), estimated from the carbon monoxide difference spectrum, varied among enzymes. Expression data are given in Table 3. Levels of expression ranged from 9 to 225 pmol P450/mg protein. With the exception of E166Q, all mutants that expressed less than 50 pmol P450/mg protein are located in the protein active-site. Levels of coexpressed CPR varied to a lesser extent, with a mean yield of 292 ± 64 pmol reductase/mg protein ($n > 60$ experiments). As noted under *Materials and Methods*, the P450/CPR ratio for the wild-type CYP1A1 and all CYP1A1 mutants was in the range of 1:1 to 1:32, which is expected to provide sufficient reductase for efficient catalysis.

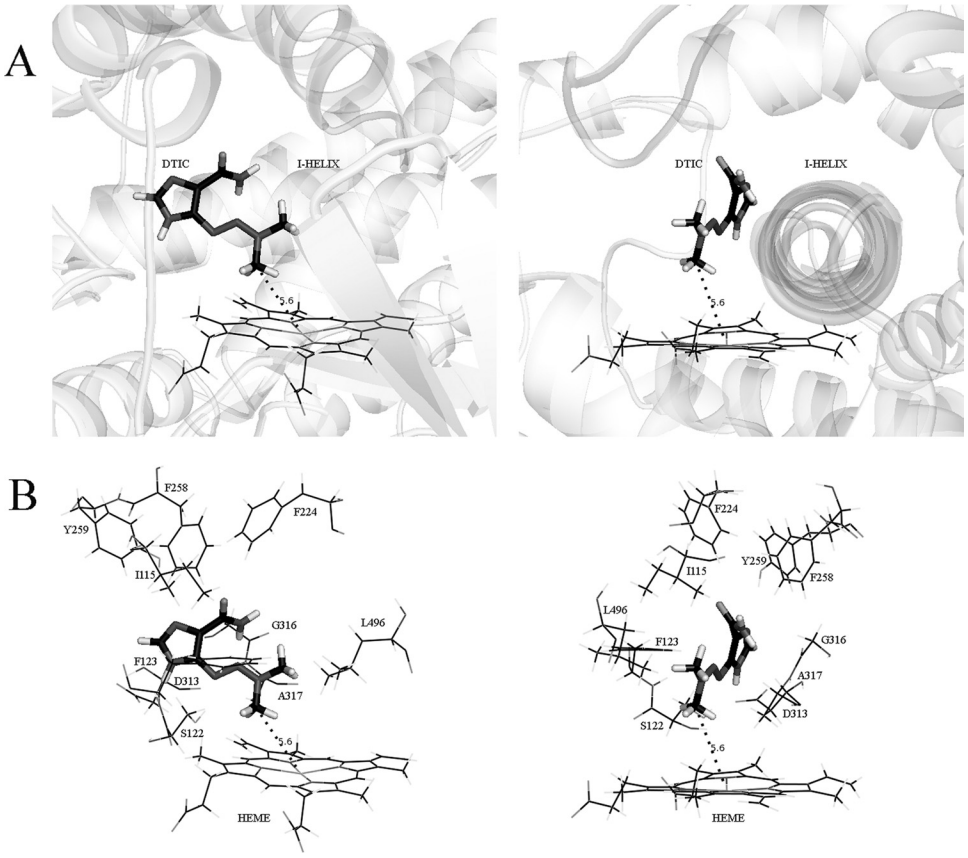

Fig. 2. Orthogonal image of the α-carbon of the *N*-dimethyl substituent positioned in the energetically favored orientation for *N*-demethylation (A) and key amino acids (lines) of CYP1A1 involved in the binding and orientation of DTIC (capped sticks) (B). Secondary structure, gray (translucent); carbon atoms, black; nitrogen atoms, dark gray; hydrogen atoms, gray.

TABLE 2

Structural data of CYP1A1 mutants with docked DTIC orientated for productive *N*-demethylation

RMSD is calculated from the Cα backbone compared with that of the wild-type CYP1A1 template. DTIC orientation is based on the distance of the α-carbon targeted for N-dealkylation from the heme iron and its angle relative to the planar heme (see *Materials and Methods*).

Mutant	RMSD	DTIC Orientation	
		°	Å
S116A	0.1307	95.2	6.2
S122A	0.0287	99.7	5.5
S122T	0.0408	115.2	4.3
F123A	0.0739	114.6	4.8
E161K	0.0718	126.3	4.3
E166Q	0.0512	105.3	5.0
V191M	0.058	106.8	4.9
F224A	0.1327	106.0	4.7
V228T	0.0978	108.2	5.8
E256K	0.0680	95.4	6.8
Y259F	0.1174	120.4	4.0
N309T	0.0631	102.8	5.7
L312F	0.0652	92.2	6.5
D313A	0.0434	101.7	4.5
D313N	0.0678	122.6	4.1
G316V	0.0449	132.6	2.9
A317G	0.0297	111.7	4.5
D320A	0.0693	102.6	5.2
T321G	0.0525	124.5	3.8
T321P	0.0728	113.8	4.3
T321S	0.0212	110.8	5.0
V322A	0.0441	119.5	4.5
I386G	0.0326	115.5	4.9
I386V	0.0359	127.1	3.9
I458P	0.0362	112.2	4.5
I458V	0.0505	106.4	4.8
T497S	0.1016	123.4	4.7

TABLE 3

Holo-P450 yields for enzymes expressed in *E. coli*

Expression levels shown as mean ± S.D. ($n \geq 3$).

Enzyme	Yield
	pmol P450/mg
CYP1A1	141 ± 8
S116A	103 ± 7
S122A	56 ± 2
S122T	61 ± 0.5
F123A	9 ± 3
E161K	94 ± 9
E166Q	33 ± 7
V191M	225 ± 9
F224A	54 ± 12
V228T	95 ± 11
E256K	115 ± 36
Y259F	115 ± 5
N309T	132 ± 2
L312F	115 ± 4
D313A	57 ± 3
D313N	35 ± 3
G316V	165 ± 13
A317G	101 ± 5
D320A	223 ± 9
T321G	59 ± 2
T321P	59 ± 12
T321S	57 ± 2
V322A	27 ± 9
I386G	22 ± 7
I386V	42 ± 32
I458P	134 ± 26
I458V	89 ± 6
T497S	84 ± 5

Effects of CYP1A1 Mutations on DTIC Activation. Wild-type CYP1A1 and mutant CYP1A1 enzymes were characterized for DTIC *N*-demethylase activity, measured as AIC formation, to generate kinetic parameters (Table 4). With the exception of the I386G mutant, all enzymes catalyzed DTIC N-demethylation. The CYP1A1 mutants S122A, S122T, F123A, E166Q, D313A, D313N, T321G, T321P, T321S, and T497S displayed negative cooperative kinetics and data were modeled using the Hill equation. Wild-type CYP1A1 and the remaining CYP1A1 mutants displayed hyperbolic rate plots, and data were well described by the Michaelis-Menten equation. It should be noted that binding of DTIC to *E. coli* membranes is <5%. Thus, variation in nonspecific binding between incubations does not account for the differences in kinetics (and kinetic parameters) observed for the CYP1A1 mutants.

Figure 3 shows representative Eadie-Hofstee plots for DTIC *N*-demethylation by wild-type CYP1A1 and the E161K, V228T, E256K, I386V, and I458V mutants. The kinetic parameters for DTIC *N*-demethylation by wild-type CYP1A1 (V_{max}, 28 ± 4 pmol · min^{-1} · pmol $P450^{-1}$; K_m, 408 ± 43 μM) are in reasonable agreement with the only other CYP1A1 data available for this substrate (V_{max} 10.2 ± 2.1 pmol · min^{-1} · pmol $P450^{-1}$; K_m, 595 ± 111 μM) (Reid et al., 1999). The E161K, E256K, and I458V substitutions all resulted in a ~2-fold increase in binding affinity (i.e., decrease in K_m) with no change in V_{max}, thereby doubling catalytic efficiency (CL_{int}) ($p < 0.05$). The V228T mutant exhibited an elevated V_{max} generating a 23% increase in CL_{int}. Although there were significant increases in both V_{max} and K_m of the I386V mutant ($p < 0.05$), there was no overall change in CL_{int} ($p = 0.872$).

CL_{int} values for all other mutants were lower than for wild-type CYP1A1. Rate versus substrate concentration and Eadie-Hofstee plots for these mutants are provided in Supplemental Fig. S1. It is noteworthy that 10 of the mutations resulted in a change from the hyperbolic kinetics observed for wild-type CYP1A1 to negative cooperative kinetics (Table 4; Supplemental Fig. S1).

TABLE 4
Derived kinetic parameters for DTIC N-demethylase activity by wild-type CYP1A1 and mutant CYP1A1 enzymes

Enzyme	V_{max}	K_m or S_{50}	V_{max}/K_m	Hill Coefficient
	pmol · min^{-1} · pmol $P450^{-1}$	*μM*	*μL · min^{-1} · pmol $P450^{-1}$*	
CYP1A1[a]	28 ± 4	408 ± 43	0.069	
S116A	26.7	412	0.065	
S122A[b]	59.9	94,332		0.50
S122T[b]	23.3	1132		0.70
F123A[b]	16.1	5237		0.80
E161K[a]	**30 ± 5**	**249 ± 22***	**0.120***	
E166Q[b]	34.8	1492		0.80
V191M	23	501	0.046	
F224A	31.4	468	0.067	
V228T[a]	**32.4 ± 1.5**	**386 ± 22**	**0.090**	
E256K[a]	**29 ± 3**	**238 ± 32***	**0.121***	
Y259F	25.9	1082	0.024	
N309T	33.9	533	0.064	
L312F	32.7	773	0.042	
D313A[b]	35.8	8749		0.80
D313N[b]	17.5	9990		0.80
G316V	19.7	6963	0.003	
A317G[c]	21.1	12,207	0.001	
D320A	18.3	1091	0.017	
T321G[b]	8.7	1117		0.70
T321P[b]	23.1	2543		0.75
T321S[b]	56.9	3119		0.60
V322A	32.2	680	0.047	
I386G	N.D.	N.D.	N.D.	N.D.
I386V[a]	**44.2 ± 4***	**765 ± 30***	**0.058**	
I458P	33.1	587	0.056	
I458V[a]	**22 ± 4**	**183 ± 61***	**0.118***	
T497S[b]	33.5	1250		0.85

N.D., not detectable.
*$P < 0.05$ compared to the corresponding parameter for the wild-type.
[a] K_m and V_{max} values are given as the mean ± S.D. of four experiments.
[b] Data from fitting with the Hill equation.
[c] The kinetic model could not be characterized.

Kinetic and Structural Analysis of DTIC Activation by CYP1A1 Enzymes. With the exception of F123A, D313N, and T321G mutants, V_{max} values for DTIC N-demethylation (measured as AIC formation) were either equivalent to or greater than those of wild type (Table 4). However, profound effects on K_m/S_{50} were observed for a number of mutants, in particular S122A, F123A, E166Q, D313A, D313N, G316V, A317G, T321P, and T321S (Table 4). The derived S_{50} value for the S122A mutant was very high, most likely because of the misalignment of DTIC in the CYP1A1 active-site, which is also due in part to the aromatic and polar interactions contributed from Tyr259 (Fig. 4A). Substitution to threonine (S122T) resulted in a smaller increase in S_{50} (Table 4), suggesting that the polar nature of residue 122 contributes significantly to binding affinity. Data obtained for the F123A mutant revealed decreases in both V_{max} and substrate binding affinity, most likely as a result of substrate destabilization caused by the loss of edge-to-face electrostatic interactions (Fig. 4B). The decrease in binding affinity observed for the E166Q substitution may arise from effects on efficient electron transfer, because residue is located in the D-helix on the outer surface of CYP1A1 (Supplemental Video V1) and may influence the interaction between CYP1A1 and CPR (Fig. 4C). The D313A and D313N mutants exhibited similar increases in S_{50}. Substrate binding affinity is presumably reduced as a result of the altered charge, which is negative to neutral at physiological pH. However, whereas replacement of the charged aspartate with asparagine significantly decreased V_{max} (Fig. 4D), substitution with alanine resulted in a small increase in this parameter relative to wild type. Residues 316 and 317 are located in the I-helix (Fig. 4E). The G316V and A317G substitutions alter the volume of the active-site and affect the optimal alignment of DTIC for productive N-demethylation. Both substitutions alter conformation of the I-helix, but there is a more substantial effect on substrate binding affinity from removal of the side-chain at residue 317 (A317G).

Residue 321 is located in the I-helix and is highly conserved (96.6%) among human P450 enzymes (Fig. 4F). Threonine 321 is believed to facilitate proton transport during catalysis by aligning water in the "proton transfer groove" (Haines et al., 2001; Lewis et al., 2004). The decrease in activity observed for the T321G mutant may arise from altered conformational flexibility in the I-helix and/or effects on the alignment of water in the active-site. Glycine and serine substitutions at residue 321 relieve the restricted secondary structure as a result of the β-branched side-chain of threonine in the wild-type enzyme. In the case of the T321P mutant, the restricted geometry ($\psi = -75°$) ensures that this residue behaves as a β-branched amino acid, with a substantial impact on substrate binding affinity.

Discussion

Although DTIC has relatively poor clinical activity and results in numerous adverse effects, it is still the most effec-

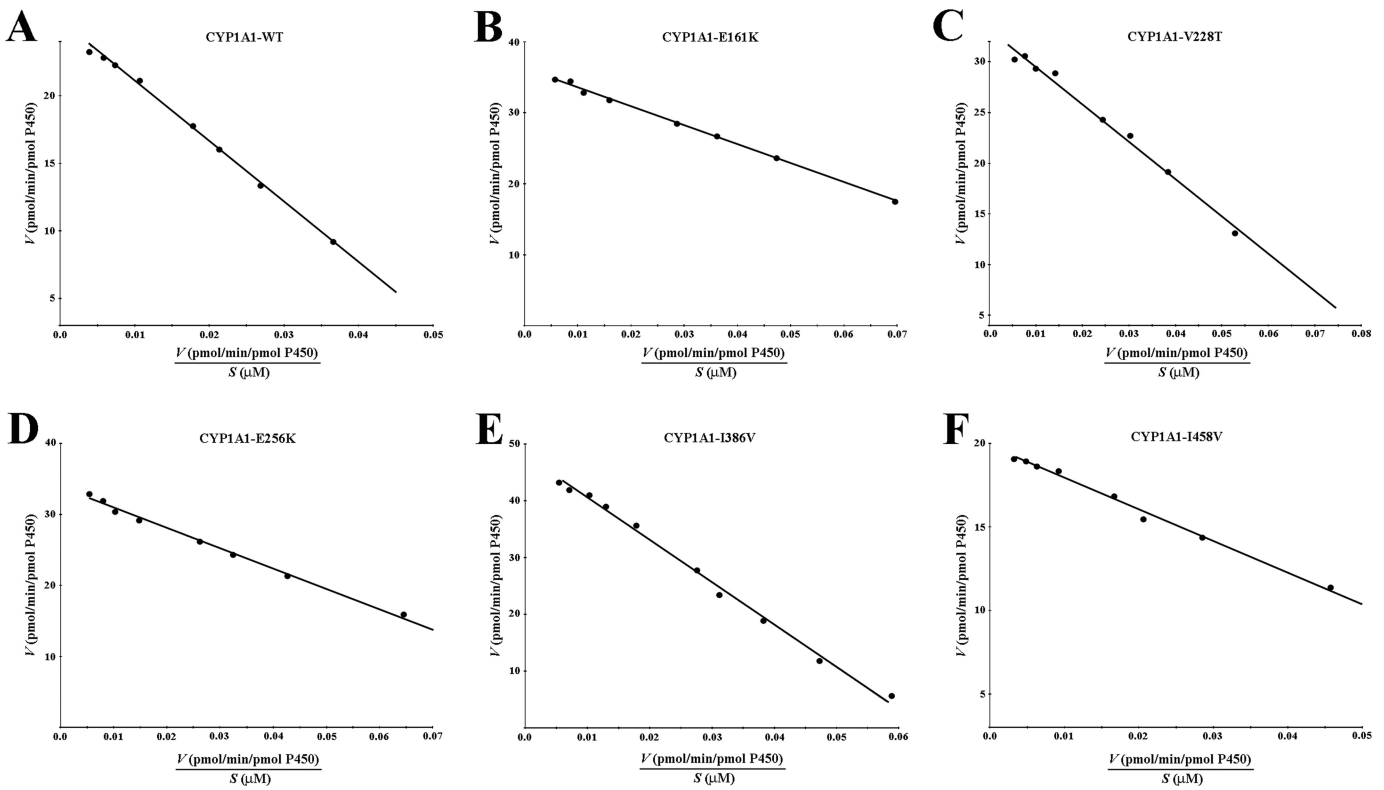

Fig. 3. Eadie-Hofste plots for DTIC N-demethylation by wild-type CYP1A1 (A), CYP1A1-E161K (B), CYP1A1-V228T (C), CYP1A1-E256K (D), CYP1A1-I386V (E), and CYP1A1-I458V (F). Points show experimentally determined activities; lines are from model-fitting.

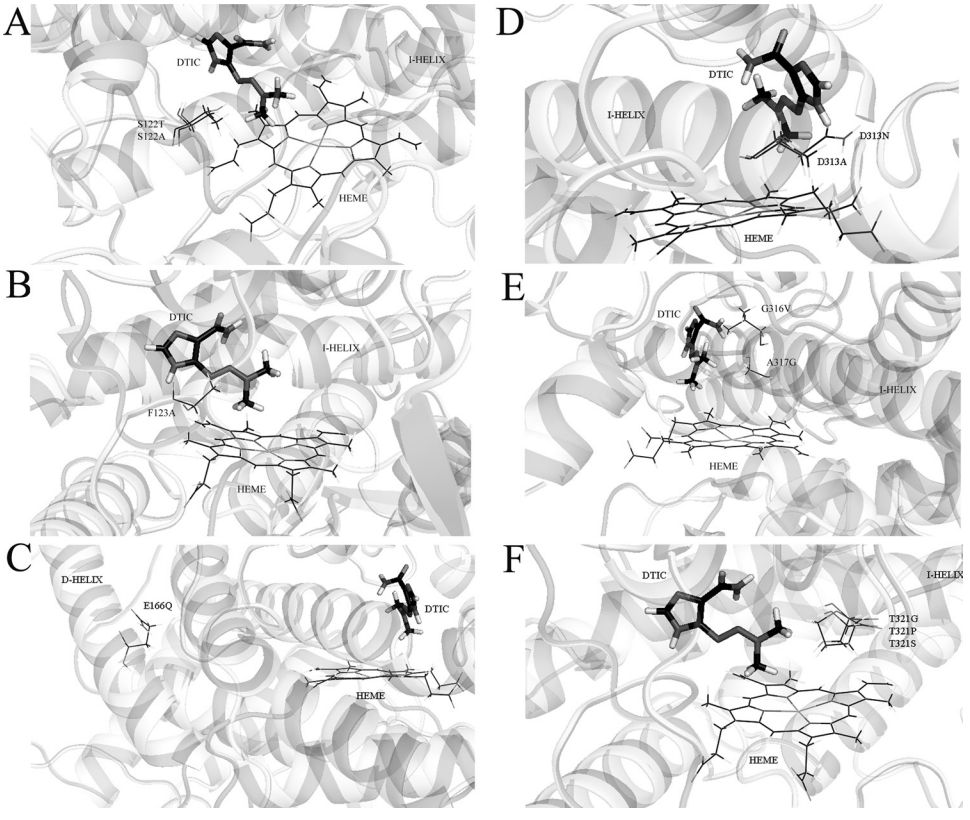

Fig. 4. Structural orientations of key mutations. A, CYP1A1-S122A/S122T; B, CYP1A1-F123A; C, CYP1A1-E166Q; D, CYP1A1-D313A/D313N; E, CYP1A1-G316V/A317G; F, CYP1A1-T321G/T321P/T321S. Mutant residues (lines) are displayed relative to DTIC docked in the wild-type CYP1A1 structure (capped sticks). Secondary structure, gray (translucent); carbon atoms, black; nitrogen atoms, dark gray; hydrogen atoms, gray.

tive single agent used for the treatment of metastatic malignant melanoma (Erdmann, 2010). Although the pharmacology of DTIC is well understood, only a single study has investigated the metabolism of DTIC by cytochromes P450 (Reid et al., 1999). Given that DTIC requires metabolic activation by P450s for cytotoxicity, an opportunity exists to use mutant enzymes with enhanced DTIC activation for potential use in P450-based GDEPT strategies.

Docking studies revealed DTIC orients near Ser122, Phe123, Asp313, Ala317, Ile386, Tyr259, and Leu496 (Fig. 2B). The energetically favorable pose placed the hydroxylated carbon 5.6 Å from the heme catalytic site, with H-bonding occurring between Tyr259 and the aromatic nitrogen of the imidazole ring (Fig. 2, A and B). In addition to Tyr259, H-bonding interactions of mutant enzymes occurred at positions 122, 313, and 316 and were dependent on the type of amino acid substituted. It is noteworthy that the energetically favored orientation of DTIC in the E256K mutant revealed H-bonding not only from N^2 of the imidazole but also from the carboxamide to Tyr259. Based on the predictivity of the CYP1A1 model (Lewis et al., 2007), DTIC binding and orientation was assessed with mutants generated in silico. All mutants were designed to alter the *N*-demethylation of DTIC by manipulating steric, polar, aromatic, or electrochemical interactions.

To determine the effect of each mutation on the conversion of DTIC to AIC (via N-demethylation), the coexpression of recombinant CYP1A1 proteins with CPR was achieved using an optimized method that increased yield 7-fold compared with literature reports (Table 3). All enzymes catalyzed DTIC N-demethylation except for the I386G mutant, despite the presence of holo-P450. The lack of both DTIC N-demethylation and 7-ethoxyresorufin *O*-deethylation (Lewis et al., 2007) suggests that flexibility in the K-helix/β2-3 loop may affect the substrate access channel/active-site boundary. The CYP1A1 computational model identified that Phe123 relaxes into a void in the CYP1A1 substrate access channel generated by the I386G mutant. The aromatic side-chain of Phe123 pivots inward toward the heme prosthetic group by 25.4°. Although the distance between Phe123 and Ile386 in the wild-type protein (3.1 Å) is the same as that between Phe123 and Gly386 in the mutant, the decrease in side-chain size (−2.2 Å) and loss of β-branching results in constriction at the CYP1A1 substrate access channel/active-site boundary. Proline 387 is similarly affected by the glycine substitution in the I386G mutant, resulting in disruption of the architecture of the substrate-access channel. However, this effect is not sufficient to hinder heme incorporation during protein folding or the access of $CO_{(g)}$.

The kinetics of AIC formation (via DTIC N-demethylation) by CYP1A1 was well modeled using the Michaelis-Menten equation (Fig. 3). DTIC N-demethylation by the E161K, E256K, and I458V mutants similarly exhibited Michaelis-Menten kinetics, with lower K_m values that resulted in a doubling of catalytic efficiencies (Table 4). The V228T mutant increased catalytic efficiency relative to the wild-type enzyme by 23%. The mechanism(s) associated with the altered substrate binding affinity differs for each of these high-activity mutants. Although it is difficult to elucidate structure-activity relationships for the E161K mutant because this residue resides on the surface of the protein (Fig. 4A; Supplemental Video V1), the substitution of glutamate for lysine results in a reversal in charge-state of the substituted amino acid, with a change in protonation at physiological pH. It is believed that residue 161 is involved in CPR binding (Parikh et al., 1999). Thus, the localized charge effects seen with the E161K substitution may aid a more complementary alignment of CPR via salt-bridge formation. For the E256K mutant, localized charge effects enhance H-bonding to D253 (Fig. 5). Of particular interest were modifications in the side-chain orientations of Phe258 and Tyr259, which affect DTIC alignment over the heme catalytic site. The decrease in K_m obtained with the I458V mutant apparently results from realignment of the heme prosthetic group. Preservation of Cβ-branching maintains the rigid conformation of the β4-2/L-helix loop and improves activity (Table 4).

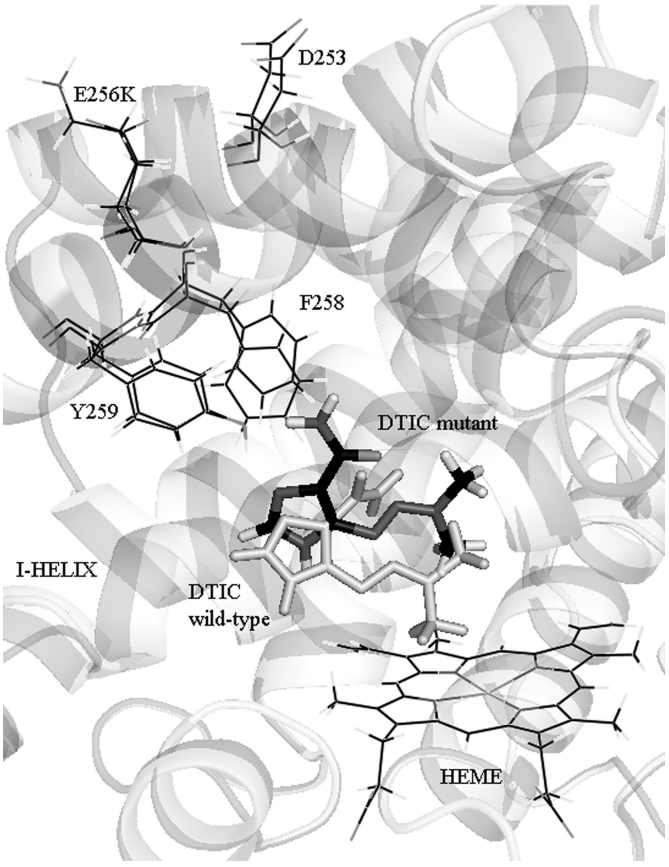

Fig. 5. The E256K substitution modifies the side-chain orientation of Phe258 and Tyr259 (lines), which alters DTIC (capped sticks) alignment compared with the wild-type CYP1A1 enzyme (gray capped sticks). Secondary structure, gray (translucent); carbon atoms, black; nitrogen atoms, dark gray; hydrogen atoms, gray.

Although the primary focus of this study was to generate CYP1A1 enzymes with enhanced DTIC *N*-demethylase activities (measured as AIC formation), data obtained for other mutants contribute to the overall understanding of CYP1A1 structure-activity relationships. Although the S122A, D313A, and T321S mutants showed higher V_{max} values for DTIC *N*-demethylation compared with wild-type CYP1A1, there were large decreases in binding affinity (assessed as S_{50}) (Table 4; Supplemental Fig. S1). In addition, all three mutants exhibited negative cooperative kinetics. It is noteworthy that a doubling in V_{max} and reduction in binding affinity was similarly observed for 7-ethoxyresorufin *O*-deethylation by S122A (Lewis et al., 2007). Docking studies with 7-ethoxyresorufin identified that hydrogen bonding of the oxazine ring oxygen to residue 122 was disrupted in the S122A mutant, resulting in a productive binding orientation where hydrogen bonding occurs between the phenoxazine carbonyl of 7-ethoxyresorufin and the hydroxyl oxygen of Tyr259. The D313A substitution in this study is expected to produce significant effects on the volume and topology of the active site, and the loss of charge associated with aspartic acid will influence interactions with neighboring resi-

dues. Although residues 122 and 313 are sufficiently distal to the catalytic heme iron to have no direct impact on reaction mechanism, they do alter the optimal alignment and orientation of the substrate for productive hydroxylation (Table 2). In contrast, residue 321 is located in the I-helix adjacent to the heme and is known to influence catalysis. Thus, V_{max} depends on the amino acid substitution; data obtained for T321G, T321P, and T321S support this notion (Table 4). In particular, substitution with the polar serine (T321S) doubled the V_{max} for DTIC *N*-demethylation, presumably by facilitating proton transfer (Table 4), whereas the T321G substitution resulted in a markedly reduced V_{max} relative to wild type. The latter observation is consistent with previous data from this laboratory with 7-ethoxyresorufin as substrate (Lewis et al., 2007).

Perturbations in the simultaneous "coming together" and ideal geometric alignment of substrate, molecular oxygen, water, and the heme iron lead to altered productivity in P450 enzymes. Thus, mutagenesis of active-site residues directly affect substrate orientation and catalytic efficiency. However, less obvious are the effects of disruption to the normally ordered packing of water molecules in the active-site which, similar to substrate, occur in parallel with the modification of active-site residues. In order for catalysis to proceed in proteins with an altered arrangement of water, substrate binding in an "open-state" conformation may be required for efficient proton delivery to the iron-dioxygen intermediate. Because the kinetic model for negative cooperativity does not distinguish between the simultaneous binding of multiple substrate molecules within a single active-site or the binding of two substrate molecules to two distinct binding sites (Houston and Galetin, 2005), it might be speculated that the negative cooperative kinetics observed for some mutant CYP1A1 enzymes arises from an energetically unfavored "open" conformation that subsequently allows the binding of a second substrate molecule, either within the active site or at another distinct binding site. This effect may be more prominent in P450 enzymes with small active-site cavities, such as CYP1A1 (~339 $Å^3$), which in a catalytically "closed" conformation can only accommodate a single substrate molecule in the active site. It is noteworthy that in silico docking experiments show binding of a second DTIC molecule is permitted within the substrate access channel as a result of interactions with Val228, Asn232, Ser247, and Phe251 (data not shown). Whether the "atypical" (i.e., non–Michaelis-Menten) DTIC kinetics observed here for several of the CYP1A1 mutants arises from binding within the substrate access channel or from another mechanism has yet to be established.

As noted above, it is well established that mutation of amino acids within a 3-Å radius of bound substrate is likely to affect catalytic efficiency. However, more subtle manipulation of amino acids may also enhance the catalytic activity of an enzyme-substrate pair. It is evident from data presented here that side-chain reorientation of the native active-site residues can be introduced by the mutagenesis of residues outside of the active site, and this may be achieved by consideration of the physicochemical, bonding, and folding interactions of the amino acid targeted for substitution and with the residue(s) within the active site. This process, which is also dependent on the chemical and physicochemical features of the substrate, can be facilitated by the use of a validated homology model generated from crystal templates of high quality and homology (in this case CYP1A1 and CYP1A2) and should therefore translate to other enzyme-substrate combinations. Application of the CYP1A1 homology model in this study has provided insights into the mechanism of altered kinetic parameters for DTIC *N*-demethylation. The homology model does not, however, provide a clear explanation for the negative cooperative kinetics associated with a number of the mutants.

In conclusion, this study has demonstrated that E161K, V228T, E256K, and I458V substitutions in human CYP1A1 can enhance the catalytic efficiency of DTIC activation via the N-demethylation pathway. The combination of kinetic analyses with in silico docking has permitted interpretation of the structure-activity relationships of this enzyme-substrate pair, highlighting the importance of electrostatic and charge interactions. The improved understanding of DTIC activation by CYP1A1 provides a potential strategy for CYP1A1-based GDEPT for the treatment of metastatic malignant melanoma.

Authorship Contributions

Participated in research design: Lewis, Mackenzie, and Miners.
Conducted experiments: Lewis.
Wrote or contributed to the writing of the manuscript: Lewis, Mackenzie, and Miners.

References

Aghi M, Hochberg F, and Breakefield XO (2000) Prodrug activation enzymes in cancer gene therapy. *J Gene Med* **2:**148–164.

Baldwin A, Huang ZQ, Jounaidi Y, Waxman DJ (2003) Identification of novel enzyme-prodrug combinations for use in cytochrome P450-based gene therapy for cancer. *Arch Biochem Biophys* **409:**197–206.

Daly AK (2003) Pharmacogenetics of the major polymorphic metabolizing enzymes. *Fundam Clin Pharmacol* **17:**27–41.

Denny WA (2003) Prodrugs for Gene-Directed Enzyme-Prodrug Therapy (Suicide Gene Therapy). *J Biomed Biotechnol* **2003:**48–70.

Erdmann MK (2010) Immunity unleashed in melanoma. *Lancet Oncology* **11:**108–109.

Ericksen SS and Szklarz GD (2005) Regiospecificity of human cytochrome P450 1A1-mediated oxidations: the role of steric effects. *J Biomol Struct Dyn* **23:**243–256.

Ferguson MJ, Ahmed FY, and Cassidy J (2001) The role of pro-drug therapy in the treatment of cancer. *Drug Resist Updat* **4:**225–232.

Gillam EM, Baba T, Kim BR, Ohmori S, and Guengerich FP (1993) Expression of modified human cytochrome P450 3A4 in *Escherichia coli* and purification and reconstitution of the enzyme. *Arch Biochem Biophys* **305:**123–131.

Haines DC, Tomchick DR, Machius M, and Peterson JA (2001) Pivotal role of water in the mechanism of P450BM-3. *Biochemistry* **40:**13456–13465.

Houston JB and Galetin A (2005) Modelling atypical CYP3A4 kinetics: principles and pragmatism. *Arch Biochem Biophys* **433:**351–360.

Kan O, Griffiths L, Baban D, Iqball S, Uden M, Spearman H, Slingsby J, Price T, Esapa M, Kingsman S, et al. (2001) Direct retroviral delivery of human cytochrome P450 2B6 for gene-directed enzyme prodrug therapy of cancer. *Cancer Gene Therapy* **8:**473–482.

Lewis BC, Mackenzie PI, and Miners JO (2007) Comparative homology modeling of human cytochrome P4501A1 (CYP1A1) and confirmation of residues involved in 7-ethoxyresorufin O-deethylation by site-directed mutagenesis and enzyme kinetic analysis. *Arch Biochem Biophys* **468:**58–69.

Lewis DF (2003) Essential requirements for substrate binding affinity and selectivity toward human CYP2 family enzymes. *Arch Biochem Biophys* **409:**32–44.

Lewis DF, Modi S, and Dickins M (2002) Structure-activity relationship for human cytochrome P450 substrates and inhibitors. *Drug Metab Rev* **34:**69–82.

Lewis DF, Lake BG, and Dickins M (2004) Quantitative structure-activity relationships within a homologous series of 7-alkoxyresorufins exhibiting activity towards CYP1A and CYP2B enzymes: molecular modelling studies on key members of the resorufin series with CYP2C5-derived models of human CYP1A1, *CYP1A2, CYP2B6 and CYP3A4. Xenobiotica* **34:**501–513.

Liu J, Ericksen SS, Sivaneri M, Besspiata D, Fisher CW, and Szklarz GD (2004) The effect of reciprocal active site mutations in human cytochromes P450 1A1 and 1A2 on alkoxyresorufin metabolism. *Arch Biochem Biophys* **424:**33–43.

Löhr M, Hoffmeyer A, Kröger J, Freund M, Hain J, Holle A, Karle P, Knöfel WT, Liebe S, Müller P, et al. (2001) Microencapsulated cell-mediated treatment of inoperable pancreatic carcinoma. *Lancet* **357:**1591–1592.

Lowry OH, Rosenbrough NJ, Farr L, and Randall RJ (1951) Protein measurement with the folin phenol reagent. *J Biol Chem* **193:**267–275.

Luce JK, Thurman WG, Isaacs BL, and Talley RW (1970) Clinical trials with the antitumor agent 5-(3,3-dimethyl-1-triazeno)imidazole-4-carboxamide(NSC-45388). *Cancer Chemother Rep* **54:**119–124.

Meer L, Janzer RC, Kleihues P, and Kolar GF (1986) In vivo metabolism and reaction with DNA of the cytostatic agent, 5-(3,3-dimethyl-1-triazeno)imidazole-4-carboxamide (DTIC). *Biochem Pharmacol* **35:**3243–3247.
Miles CS, Ost TW, Noble MA, Munro AW, and Chapman SK (2000) Protein engineering of cytochromes P-450. *Biochim Biophys Acta* **1543:**383–407.
Omura T and Sato R (1964a) The carbon monoxide-binding pigment of liver microsomes: Evidence for its hemoprotein nature. *J Biol Chem* **239:**2370–2378.
Omura T and Sato R (1964b) The carbon monoxide-binding pigmentof liver microsomes. *J Biol Chem* **239:**2379–2385.
Parikh A, Josephy PD, and Guengerich FP (1999) Selection and characterization of human cytochrome P450 1A2 mutants with altered catalytic properties. *Biochemistry* **38:**5283–5289.
Reid JM, Kuffel MJ, Miller JK, Rios R, and Ames MM (1999) Metabolic activation of dacarbazine by human cytochromes P450: the role of CYP1A1, *CYP1A2, and CYP2E1. Clin Cancer Res* **5:**2192–2197.
Ridderström M, Zamora I, Fjellström O, and Andersson TB (2001) Analysis of selective regions in the active sites of human cytochromes P450, 2C8, 2C9, 2C18, and 2C19 homology models using GRID/CPCA. *J Med Chem* **44:**4072–4081.
Rooseboom M, Commandeur JN, and Vermeulen NP (2004) Enzyme-catalyzed activation of anticancer prodrugs. *Pharmacol Rev* **56:**53–102.
Sanada M, Takagi Y, Ito R, and Sekiguchi M (2004) Killing and mutagenic actions of dacarbazine, a chemotherapeutic alkylating agent, on human and mouse cells: effects of Mgmt and Mlh1 mutations. *DNA Repair* **3:**413–420.
Schwarz D, Kisselev P, Ericksen SS, Szklarz GD, Chernogolov A, Honeck H, Schunck WH, and Roots I (2004) Arachidonic and eicosapentaenoic acid metabolism by human CYP1A1: highly stereoselective formation of 17(R),18(S)-epoxyeicosatetraenoic acid. *Biochem Pharmacol* **67:**1445–1457.
Shen AL, Porter TD, Wilson TE, and Kasper CB (1989) Structural analysis of the FMN binding domain of NADPH-cytochrome P-450 oxidoreductase by site-directed mutagenesis. *J Biol Chem* **264:**7584–7589.
Stevens MF, Hickman JA, Langdon SP, Chubb D, Vickers L, Stone R, Baig G, Goddard C, Gibson NW, and Slack JA (1987) Antitumor activity and pharmacokinetics in mice of 8-carbamoyl-3-methyl-imidazo[5,1-*d*]-1,2,3,5-tetrazin-4(3H)-one (CCRG 81045; M & B 39831), a novel drug with potential as an alternative to dacarbazine. *Cancer Res* **47:**5846–5852.
Xu G and McLeod HL (2001) Strategies for enzyme/prodrug cancer therapy. *Clin Cancer Res* **7:**3314–3324.
Yasukochi Y and Masters BS (1976) Some properties of a detergent-solubilized NADPH-cytochrome c(cytochrome P-450) reductase purified by biospecific affinity chromatography. *J Biol Chem* **251:**5337–5344.
Zheng L, Baumann U, and Reymond JL (2004) An efficient one-step site-directed and site-saturation mutagenesis protocol. *Nucleic Acids Res* **32:**e115.

Address correspondence to: Prof. John Miners, Department of Clinical Pharmacology, Flinders University School of Medicine, Flinders Medical Centre, Bedford Park, SA 5042, Australia. E-mail: john.miners@flinders.edu.au